Eur. Phys. J. B **10**, 663–672 (1999)

THE EUROPEAN PHYSICAL JOURNAL B

EDP Sciences

Swelling behavior and viscoelasticity of ultrathin grafted hyaluronic acid films

A. Albersdörfer[a] and E. Sackmann

Biophysics Laboratory, Physik-Department (E22), Technische Universität München, James-Franck-Straße, 85748 Garching, Germany

Received 10 September 1998 and Received in final form 30 November 1998

Abstract. In this paper we study the effect of monovalent Na^+ and divalent Ca^{2+} ions on the swelling behavior and viscoelastic parameters of ultrathin layers of the natural polyelectrolyte hyaluronic acid covalently coupled to glass substrates. A colloidal probe technique is applied for this purpose based on μm latex beads, hovering over the polymer cushion. By analyzing the vertical Brownian motion of these beads with reflection interference contrast microscopy (RICM) we determined the equilibrium layer thickness (with 3 nm vertical resolution), the interfacial interaction potential, and the characteristic mesh size limiting the hydrodynamic flow within the polyelectrolyte film as a function of the ionic strength. The experimental results are interpreted in terms of three different theoretical models: the polyelectrolyte brush approximation of Pincus [1], a modified polyelectrolyte brush approximation in the high salt concentration limit of Ross and Pincus [2] and the simple scaling approximation for neutral adsorbed polymers of de Gennes [3]. Within experimental error all of these different models fit our experimental data and yield comparable results for the equilibrium layer thickness. Moreover we determine a thickness dependent, effective surface coverage from both brush models. The hydrodynamic properties of the films are interpreted in terms of the Brinkmann model of elastic porous media by assuming an effective mesh size, which depends linearly on the Debye screening length. The salt induced condensation of the polyelectrolyte films can be described microscopically in terms of a progressive contraction of the mesh size with increasing salt concentration.

PACS. 36.20.Ey Conformation (statistics and dynamics) – 61.25.Hq Macromolecular and polymer solutions; polymer melts; swelling – 83.80.Lz Biological materials: blood, collagen, wood, food, etc.

1 Introduction

Hyaluronic acid is a linear, anionic polysaccharide that occurs in many living substrates as synovial fluid, the skin, cartilage, umbilical cord, or the vitreous humor of the eye. It is the major component of the extra cellular matrix that surrounds migrating and proliferating cells, particularly in embryonic tissue [4]. The physical forces resulting from hyaluronic acid swelling are supposed to contribute to early neuronal morphogenesis. Many studies have suggested that accumulation of hyaluronic acid confined in the extra cellular matrix between cells can generate local disjoining pressure creating hydrated pathways by separating the cellular barriers. This process is essential for the development of the neural tube [5]. Furthermore hyaluronate has attracted much attention in the biomedical field. For example, hyaluronan can be used to replace the vitreous fluid during opthalmic surgery [6]. Moreover, hyaluronate that acts like a lubricant and a shock absorber in the joint can be injected directly into the knee of patients with osteoarthritis to complete the body's own hyaluronic acid.

The biological role of hyaluronic acid is especially fascinating from a physical point of view because its functionality can mostly be traced back to the viscoelastic properties of polyelectrolyte networks. The open, random coil structure of hyaluronic acid exhibits large solvent domains due to the large number of hydrophilic residues. This gives hyaluronic acid, even at low concentrations, the character of a high viscosity hydrogel, which is responsible for its outstanding lubrication properties [7]. Moreover, hyaluronic acid imparts stiffness and resiliency due to the well-known entropic elasticity of polyelectrolytes. Owing to the large number of charged residues the state of hyaluronic acid is very sensitive to the ionic content in the solution.

In this work we demonstrate that the change in local structure of the polyelectrolyte chains leads to a remarkable swelling and condensation behavior of grafted hyaluronic acid films when the salt concentration is changed. We also studied the viscoelasticity of the grafted layer under different solvent conditions. To determine the viscoelastic parameters we analyzed the Brownian motion of latex beads in the interaction potential generated by superposition of gravity and the repulsion

[a] e-mail: aalbersd@ph.tum.de

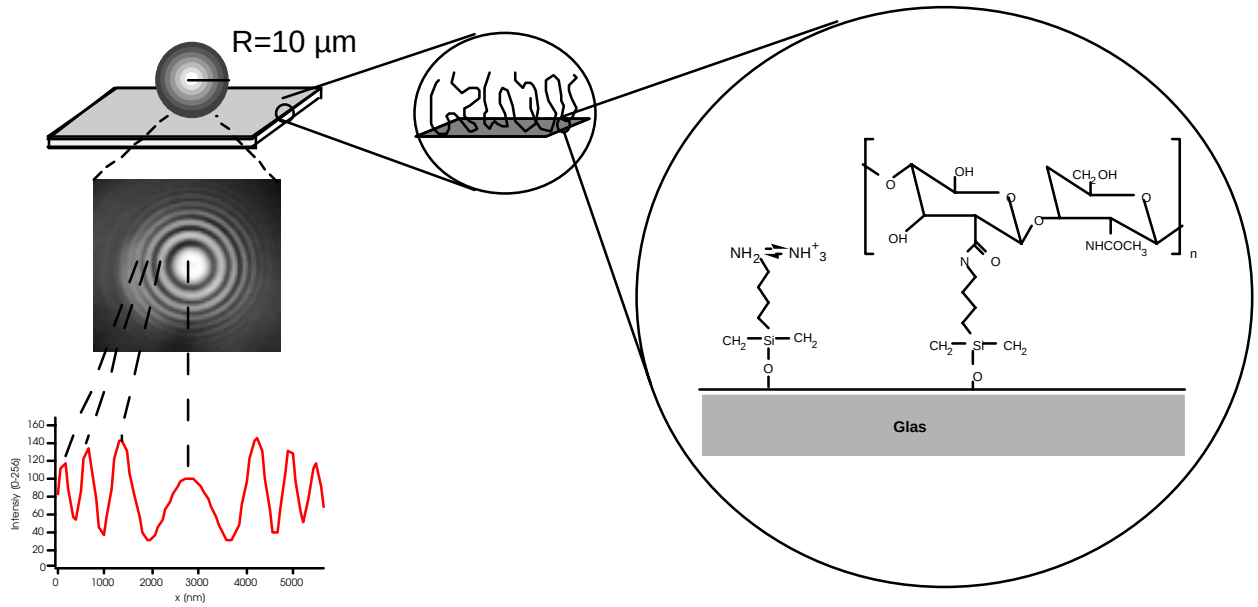

Fig. 1. Left: schematic view of the measuring principle. A latex bead interacting with the substrate is used as colloidal probe. The sphere-substrate distance is determined by evaluating the RICM image of the lower cap of the sphere. Also shown is a typical intensity profile of a crossection through the center of the interference pattern. Right: the insert shows the chemical structure of a hyaluronic acid monomer coupled to the amino-silanized glass substrate.

of the polyelectrolyte network. This method was recently developed in the author's laboratory [8] and applied to neutral polymer films by Kühner and Sackmann [9].

2 Materials and methods

2.1 Hyaluronic acid

Bacterial hyaluronic acid from streptococcus zooepidemicus was purchased from Aldrich (Aldrich Chemie GmbH, Steinheim, Germany). It is a water soluble polyanionic macromolecule consisting of up to 10^4 repeating disaccharide units of N-acetyl-D-glycosamine and D-glycuronic acid (Fig. 1, right side) which is dissociated under physiological pH conditions ($pK_s = 3.21$ [9]) yielding a charge parameter of $f = 0.7$ (charges per monomer unit) [11]. The average molecular weight of bacterial hyaluronic acid was found to be up to several 10^6 Da [12] corresponding to an extended length of ~ 10 μm. Based on light scattering and intrinsic viscosity measurements persistence lengths smaller than 8 nm were found in the high ionic strength limit [13]. As each disaccharide unit is approximately 1 nm in length the persistence length corresponds to only 8 individual monomer subunits. This corresponds to a high degree of molecular flexibility that makes random coil approximations reasonable.

2.2 Sample preparation

2.2.1 Silanization

Glass cover slides (24 mm × 24 mm, AL, Germany) were cleaned by successive ultrasonification, first two times in a 2 vol% aqueous solution of Hellmanex (Hellma GmbH, Mühlheim, Germany), and second, two times in Millipore filtered water (Millipore Milli-Q-System, Molsheim, France), for 30 min, respectively. Between each sonification step the glass slides were rinsed about 10 times with Millipore water. After this cleaning procedure the glass slides were dried for several hours at 75 °C. Thereafter the clean and dry substrates were silanized with 4-amino butyl-dimethyl-mono-methoxysilane (ABDMS) purchased from ABCR (ABCR GmbH, Karlsruhe, Germany). The ABDMS was deposited as described previously [14,15]. In brief: the substrates were placed in a teflon holder that was deposited in a glass flask. 0.2 ml of ABDMS were dropped into the flask. The flask was evacuated to 20 mbar and then heated to 150 °C for two hours. Silane was evaporated, and the silanization occurs from the gas phase. After the silanization the samples were rinsed with chloroform to remove unbound ABDMS leaving a homogeneous and correctly oriented aminosilane layer [16].

2.2.2 Hyaluronic acid anchoring

To couple the polymer to the substrates 1.0 mg/ml hyaluronic acid was solved in 10 mM 4-(2-hydroxyehtyl)-piperazine-1-ethane sulfonic acid-buffer (HEPES, Fluka GmbH, Neu Ulm, Germany) at pH 7. Then 0.2 M N-(3-dimethyl amino propyl)-3-ethyl carbodiimide hydrochloride (EDC, Aldrich Chemie GmbH, Steinheim, Germany) and 0.05 M N-hydroxysuccinimide (NHS, Fluka GmbH, Neu Ulm, Germany) were added to functionalize the carboxyl groups with active esters. Five minutes later the glass slides, functionalized with aminosilane, were immersed into the activated hyaluronate solution for 12 h

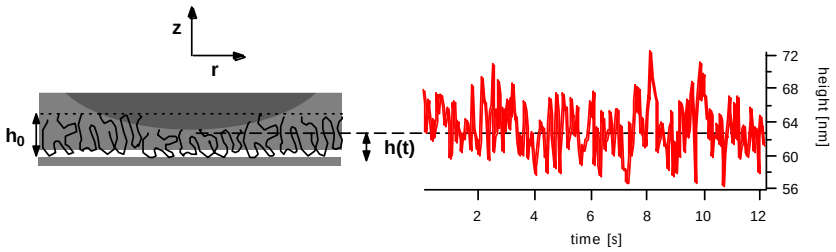

Fig. 2. Left: geometry of a sphere hovering over a polymer covered glass slide with $h(t)$ the time dependent sphere-substrate distance and h_0 the equilibrium layer thickness. Right: example of thermal height fluctuations around the mean sphere-substrate distance.

at room temperature. Finally the freshly prepared substrates were washed in Millipore filtered water for at least one week, while shaking the glass slides on an incubator table and daily exchanging the water. This washing procedure ensures that only covalently bound hyaluronic acid remains at the surface.

The success of each of the preparation steps can easily be checked by the different wettability of the different substrates with water. Additionally the film thickness on thermally oxidized silicon wafers (Wacker Chemietronic GmbH, Burghausen, Germany) which were prepared simultaneously in the same way was measured by ellipsometry to control the silanization and the hyaluronic acid deposition.

2.3 Experimental method

We measured the time dependent height of microscopic latex beads above grafted polyelectrolyte films using reflection interference contrast microscopy (RICM). Latex beads with a specific density of 1.05 g/cm^3 [17], a refractive index of about 1.55, and typical values for the radius between 8 and 10 μm were purchased from polysciences (polysciences Inc., Warrington, PA).

The measuring device as well as the method of quantitative analysis of RICM images were described previously [9,18]: The interference pattern resulting from the interference of light reflected from the surface of the latex bead and from the substrate, respectively (Fig. 1, left side), was analyzed using the non local theory of RICM image [9]. With this method the absolute bead-substrate distance can be measured with an accuracy of 3 nm and the deviation from the mean distance is exact to ± 0.2 nm even in the presence of silane- and polymer films [9]. In order to measure the height fluctuations of the bead the interference fringes of the RICM images were processed in real time. A tracing algorithm searches the center position of the bead and evaluates the interference pattern. For each experiment this procedure was applied to 600 images exhibiting a time distance of 40 ms. An example of the temporal height fluctuations obtained with the above procedure is shown in Figure 2. The radius of the latex bead was determined independently by bright field microscopy.

2.4 Analysis of the bead height fluctuation

The Brownian motion of a latex bead in the interaction potential $V(h)$ of the substrate is described by the Langevin equation

$$m\frac{\partial^2 h}{\partial t^2} + \frac{\partial h}{\partial t} + \frac{\partial V}{\partial t} = f_{\text{stoch}} \tag{1}$$

with h being the smallest distance between the sphere and the glass substrate, m the mass of the bead, and f_{stoch} the fluctuating force of the thermal noise. The second term is the frictional force F with the frictional coefficient γ, which can be expressed by [19].

$$\gamma = \frac{F}{\partial h/\partial t} = 6\pi R^2 \frac{\eta_{\text{eff}}}{h} \tag{2}$$

R is the radius of the latex bead, which is large, compared to h, $\partial h/\partial t$ is the relative velocity and η_{eff} is the effective shear viscosity of the surrounding medium including the polyelectrolytes grafted on the glass surface. Since $R \approx 10$ μm and $h \approx 100$ nm the latex bead is strongly overdamped and we may neglect the acceleration term $m\partial^2 h/\partial t^2$ in (1). Furthermore, the interaction potential can be harmonically approximated about its minimum since the height fluctuations $\mathrm{d}h = h - \langle h\rangle$ are small.

$$V(h) \approx V''\mathrm{d}h^2 \tag{3}$$

where V'' is the second derivative of the interaction potential which can be interpreted as an elastic force constant of the polyelectrolyte "spring". With these approximations we can calculate the autocorrelation function of the height fluctuations $\langle \mathrm{d}h(t)\mathrm{d}h(0)\rangle$. Applying the fluctuation-dissipation theorem one obtains from (1) and (2):

$$\langle \mathrm{d}h(t)\mathrm{d}h(0)\rangle \approx \frac{k_{\text{B}}T}{V''} \exp\left(-\frac{\langle h\rangle V''}{6\pi R^2 \eta_{\text{eff}}} t\right). \tag{4}$$

Since the whole system is in thermal equilibrium with its environment we can calculate also the height dependence of the interaction potential from the Boltzmann probability distribution $p(h)$ of the sphere-substrate distance:

$$\frac{V(h)}{k_{\text{B}}T} = -\ln\left[p(h)\right] + \text{const.} \tag{5}$$

3 Theoretical background

3.1 Polyelectrolyte induced forces

In order to analyze the forces arising from the hyaluronic acid layer we have to fit the measured data to a theoretical model, which describes the experimental situation correctly. Unfortunately, the layer structure, which is the basis of any theoretical description, is not known exactly in our case. The grafting procedure is expected to lead to randomly adsorbed and covalently grafted segments of the chains, which are then assumed to have a conformation with loops and free dangling ends of varying size. Since there is no theoretical model available yet for this conformation, we will describe our system in terms of different simple approximations, which involve at least partly the special structural properties of the studied layer. On the one hand it is reasonable to assume that the resulting monomer density profile resembles that of thermally adsorbed chains. On the other hand the covalent coupling leads to irreversible grafting points, which is the basis of simple theoretical models for end-grafted polyelectrolyte brushes. We therefore consider three different models for the repulsive interaction potential induced by grafted polyelectrolytes that are applied in this work: the standard Pincus model for charged brushes [1], the modified Ross and Pincus model for charged brushes [2], and the scaling approximation for adsorbed neutral polymers [3].

Pincus derived simple analytic scaling laws for the elasticity and the layer thickness of polyelectrolyte brushes. In this model the monomer concentration is assumed to be uniform throughout the layer thickness h [1]. He postulated that the dominant effect of electrostatics on polyelectrolytes is to preserve local charge neutrality at the expense of the entropy of mixing of the counterions, which is increased if they can explore larger volumes. The repulsive interaction between polyelectrolyte coated surfaces can therefore be interpreted in terms of the entropic cost associated with the localization of the counterions about the polyelectrolyte chains during compression of the brushes. Below the Manning condensation threshold [20] the counterions are not condensed and are essentially free. To a first approximation the solution can then be considered as an ideal gas of counterions of concentration fc, where c is the monomer density. In the case of a polyelectrolyte solution without added salt the osmotic pressure is $p = k_{\mathrm{B}}Tfc$. In the presence of added salt the zero-salt osmotic pressure has to be corrected by a factor, which takes into account the smaller local counterion "atmosphere" around a polyelectrolyte segment. This increase of the counterion density is accounted for by a modified Debye screening length $\kappa^{-1} = [4\pi b(c + 2n_{\mathrm{s}})]^{-1/2}$ [20] where b is the Bjerrum length and n_{s} is the salt concentration. The osmotic pressure of the polyelectrolyte layer can then be described with an effective excluded volume per monomer $v_{\mathrm{el}} \approx 4\pi b\kappa^{-2}$ [21]. This yields [1,21]

$$\frac{p}{k_{\mathrm{B}}T} \approx fc\,\frac{c}{c + 2n_{\mathrm{s}}} = \frac{f\Gamma^2}{\Gamma h + 2h^2 n_{\mathrm{s}}} \tag{6}$$

where $\Gamma = hc$ is the monomer surface density of the brush. In contrast to simple charged interfaces, where the counterions generate an exponential screening law, the disjoining pressure in the case of polyelectrolytes decays only with an algebraic power law of the electrolyte concentration.

The equilibrium brush thickness h_0 of the uncompressed brush, determined by the balance between the swelling effect of the counterion entropy and the chain elasticity, was calculated by Pincus [1] to

$$h_0 \approx (Na)^{2/3}\,(\Gamma/n_{\mathrm{s}})^{1/3} \tag{7}$$

where N is the number of monomers per chain and a is the length of the monomer.

In the high salt concentration limit Ross and Pincus [2] postulated a possible crossover to a regime in which the effective electrostatic excluded volume depends on the persistence length l_{el} according to $v_{\mathrm{el}} \approx l_{\mathrm{el}}^2\kappa^{-1}$. With the rod concentration of $c_{\mathrm{r}} = ca/l_{\mathrm{e}}$ the osmotic pressure and the equilibrium layer thickness are given by

$$\frac{p}{k_{\mathrm{B}}T} \approx \frac{1}{2}v_{\mathrm{el}}c_r^2 \approx \frac{a^2\kappa^{-1}\Gamma^2}{2h^2} \tag{8}$$

$$h_0 \approx \left(N^4a^2/b\right)^{1/6}\Gamma^{1/3}n_{\mathrm{s}}^{-1/2}. \tag{9}$$

In order to take into account the non-uniform monomer density profile we further consider a simple scaling theory for adsorbed neutral polymers as a crude approximation for randomly grafted polyelectrolytes in the high salt concentration limit [3]. The basic assumption of the adsorbed chain model is that the mesh size of the polymer network is proportional to the distance from the substrate. Following de Gennes the osmotic pressure for neutral linear polymers is

$$\frac{p}{k_{\mathrm{B}}T} = \frac{\varepsilon}{h^3} \tag{10}$$

where ε is a constant of order one.

The interaction potential $V(h)$ for the situation in Figure 2 (left side) can be calculated by integrating the pressure over the interacting surfaces using the Derejaguin approximation [22]. We assume that the surface with the grafted polyelectrolytes is flat and interacts with the smooth spherical surface of the latex bead with radius R. By making use of the azimutal symmetry we introduce cylindrical coordinates (z, r, φ), with z measured normal to the flat surface. In this coordinate system the separation between the two surfaces varies approximately as $h(r) \approx h(0) + r^2/2R$ where $h(0) \ll R$ is the distance of closest approach. Within this approximation the interaction potential $V(h)$ for the Pincus model (6) is

$$\frac{V(h)}{k_{\mathrm{B}}T} \approx \frac{\pi R\Gamma}{n_{\mathrm{s}}}\left[\Gamma\ln\left(\frac{\Gamma + 2n_{\mathrm{s}}h_0}{\Gamma + 2n_{\mathrm{s}}h}\right) + 2n_{\mathrm{s}}h\ln\left(\frac{h\,(\Gamma + 2n_{\mathrm{s}}h_0)}{h_0\,(\Gamma + 2n_{\mathrm{s}}h)}\right)\right] \tag{11}$$

for the Ross and Pincus model (8) is

$$\frac{V(h)}{k_{\mathrm{B}}T} = \frac{\pi R a^2 \Gamma^2}{(8\pi b n_{\mathrm{s}})^{1/2}} \left(\ln\left(\frac{h_0}{h}\right) + \frac{h}{h_0} - 1 \right) \tag{12}$$

and for the model of neutral adsorbed polymers (10) is

$$\frac{V(h)}{k_{\mathrm{B}}T} = \varepsilon \pi R \left(\frac{h}{h_0^2} + \frac{1}{h} - \frac{2}{h_0} \right). \tag{13}$$

3.2 Hydrodynamic lubrication forces

We now turn to the dynamic forces acting on the latex bead and consider the following situation: The sphere that is moving towards the substrate induces a dynamic transverse pressure gradient driving the fluid out of the narrow gap between the two opposite surfaces. The viscous drag of the solvent on the two bounding surfaces leads to a normal stress. In the region where the polyelectrolyte layer is not compressed by the latex bead the lubrication force is given by (see also (2)):

$$F_{\mathrm{W}} = 6\pi R^2 \frac{\partial h}{\partial t} \frac{\eta_{\mathrm{W}}}{h} \tag{14}$$

where η_{W} is the fluid shear viscosity of the bulk water.

At the bottom of the sphere, where it is immersed into the polyelectrolyte layer, viscous dissipation is enhanced dramatically because the grafted chains provide additional sources of hydrodynamic friction. Since the grafted polyelectrolytes act as fixed network we may describe the viscous drag by the Brinkmann equation [23] which approximates the polyelectrolyte layer by an elastic porous medium through which the medium flows.

$$\eta_{\mathrm{W}} \nabla^2 \mathbf{v} - \frac{\eta_{\mathrm{W}}}{\xi_{\mathrm{H}}^2(h)} \left(\mathbf{v} - \frac{\partial \mathbf{u}}{\partial t} \right) - \nabla P = 0. \tag{15}$$

The first term is the viscous stress with $\mathbf{v}$ the solvent velocity field in the polyelectrolyte film. The second term describes the friction between polyelectrolyte and solvent where $\mathbf{u}$ is the displacement field of the polyelectrolytes. ξ_{H} is the hydrodynamic screening length that depends on the local polyelectrolyte- and salt concentration. The last term is the hydrodynamic pressure gradient. Since the polyelectrolytes are fixed at the glass slide $|\mathbf{v}| \gg |\partial \mathbf{u}/\partial t|$ holds and $\partial \mathbf{u}/\partial t$ can be neglected in (15). Integration of the dynamic pressure over the immersed part of the bead's surface yields the hydrodynamic lubrication force in the region of the compressed polyelectrolyte layer [24]

$$F_{\mathrm{P}} = \pi R^2 \eta_{\mathrm{W}} \frac{\partial h}{\partial t} \int_h^{h_0} \frac{h' - h}{h' \xi_{\mathrm{H}}^2(h')} \mathrm{d}h'. \tag{16}$$

Following Rabin *et al.* [21] the height dependence of the hydrodynamic screening length can be approximated by treating the polyelectrolyte layer as a semidilute suspension of slender rods of thickness κ^{-1} and volume fraction of the rods Φ (Fig. 3a). Then the hydrodynamic screening length can be approximated by [25]

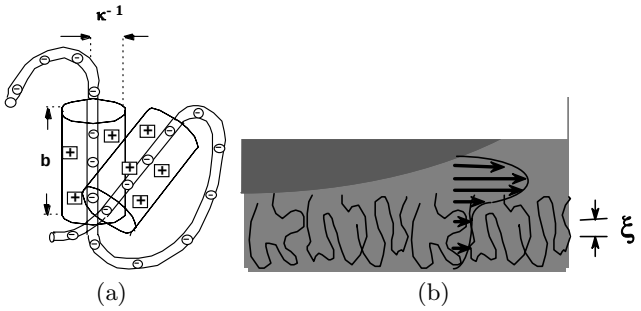

Fig. 3. (a) Local counterion atmosphere around polyelectrolyte segments. The dimension of these slender rods are defined by the Bjerrum length b and the Debye screening length κ^{-1} according to the Pincus model [1]. (b) Schematic view of the velocity field of water squeezed out of the narrow gap between substrate and approaching sphere. The flow within the layer is strongly reduced and decays with the hydrodynamic screening length ξ_{H}.

$$\xi_{\mathrm{H}} \approx \kappa^{-1} \sqrt{\frac{|\ln \Phi|}{\Phi}}. \tag{17}$$

The volume fraction of the polyelectrolyte chains in the high salt limit is given by $\Phi = 2\pi c \kappa^{-2} b$ in the Pincus model and $\Phi = 2\pi c \kappa^{-1} l_{\mathrm{el}}^2$ in the Ross and Pincus model. Neglecting the logarithmic term in (17) the hydrodynamic screening length for polyelectrolyte brushes in the high salt limit is proportional to $h^{1/2}$ for both brush models. Except for a salt concentration dependent prefactor and a logarithmic correction this is the same behavior as in the zero-added-salt case [1]. Inserting this result into (16) yields, upon integration

$$F_{\mathrm{P}} = \pi R^2 \eta_{\mathrm{W}} \frac{\partial h}{\partial t} \frac{h}{\xi_{\mathrm{H}}^2} \left(\ln\left(\frac{h_0}{h}\right) + \frac{h}{h_0} - 1 \right). \tag{18}$$

The measured damping of the bead is caused by friction in both surrounding media corresponding to (14) and (18). Since the hydrodynamic problem of the beads motion in such a system cannot be solved exactly, the measured frictional force (2) is approximated as a superposition of these two contributions $F = F_{\mathrm{W}} + F_{\mathrm{P}}$. Inserting (2), (14) and (18) into this equation yields

$$\xi_{\mathrm{H}} \approx h \sqrt{\frac{\ln(h_0/h) + h/h_0 - 1}{\eta_{\mathrm{eff}}/\eta_{\mathrm{W}} - 1}}. \tag{19}$$

3.3 Gravitational force

The gravitational potential is given by

$$V(h) = \frac{4\pi}{3} R^3 g \left(\rho_{\mathrm{latex}} - \rho_{\mathrm{water}} \right) h \tag{20}$$

where g is the gravitational acceleration.

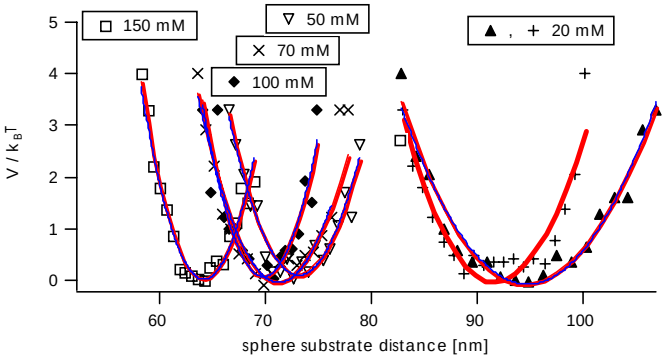

Fig. 4. Interaction potentials $V(h)$ of a latex bead sitting on a hyaluronic acid cushion in solutions with NaCl concentrations of 20, 50, 70, 100 and 150 mM. Also shown are the best fits of the data points as obtained by assuming the effective gravitational potential and three different models for the repulsive interaction potential induced by grafted polyelectrolytes: the standard Pincus model for charged brushes (—) [1], the modified Ross and Pincus model for charged brushes $(\cdots)$ [2], and the scaling approximation for adsorbed neutral polymers $(--)$ [3]. The hatched curve is the interaction potential measured in a 20 mM NaCl solution after condensation and swelling of the hyaluronic acid layer.

4 Results and discussion

4.1 The influence of monovalent ions

Figure 4 shows the interaction potentials $V(h)$ of a latex bead hovering over a hyaluronic acid cushion in buffer with NaCl concentrations between 20 and 150 mM at pH 7. All measurements were performed at room temperature and the osmolarity was controlled by freezing point depression with a commercially available osmometer. The salt concentrations were increased stepwise by exchanging the solution between the measurements carefully to maintain the lateral position of the sphere. Finally the NaCl concentration was reduced again to 20 mM in order to check the reversibility of the process. Between two measurements we let the film equilibrate for at least one hour, but it turned out that the dynamics of condensation and swelling of hyaluronic acid is faster than minutes which is the typical time scale in our experiments. Table 1 shows that the sphere-substrate distance is reduced by about 30% by increasing the ionic strength from 20 mM to 150 mM NaCl.

To interpret the presented data we make the following approximations for the relevant forces that determine the interaction potential $V(h)$. The surfaces of glass slides as well as surfaces of latex beads are supposed to have a surface charge [8]. However, in our experiments the NaCl concentrations do not fall below 20 mM corresponding to a maximum Debye screening length in the range of 3 nm. Therefore it seems reasonable to neglect electrostatic double layer forces [26] and the screened zero frequency contribution to the Van der Waals force [22] between the bare surfaces of glass substrate and latex bead. The retarded Van der Waals forces which contribute significantly only at distances smaller than 10 nm [22] do not influence the interaction potential because the sphere-substrate distance is always larger than 60 nm even at a NaCl concentration of 150 mM (*cf.* Fig. 4). For the same reason we also neglect other short-range interactions like hydration forces. In our experiments the interaction between sphere and hyaluronic acid covered glass substrate can therefore be described exclusively in terms of attractive gravitational and repulsive polyelectrolyte induced forces.

Table 1. Summary of mean sphere-substrate distance $\langle h \rangle$, equilibrium layer thickness h_0, and effective surface coverage $\Gamma_{\rm eff}$ of the grafted hyaluronic acid film obtained for different NaCl concentrations. h_0 is obtained by analyzing the data with the brush models of Pincus $(^*)$ (*cf.* (9)) and Ross and Pincus $(^{**})$ (*cf.* (10)) and the model for adsorbed neutral polymers of de Gennes $(^{***})$ (*cf.* (11)). $\Gamma_{\rm eff}$ is obtained from the two brush models.

NaCl conc./(mM)	20	50	70	100	150
$\langle h \rangle$/(nm)	94.9	73.9	71.3	69.6	63.6
$^{(*)}h_0$/(nm)	105.8	79.1	75.0	72.2	66.5
$^{(**)}h_0$/(nm)	105.9	80	75.5	72.0	66.6
$^{(***)}h_0$/(nm)	106.3	80.3	75.8	72.3	66.6
$^{(*)}\Gamma_{\rm eff}/({\rm nm}^{-2})$	0.01	0.024	0.027	0.033	0.036
$^{(**)}\Gamma_{\rm eff}/({\rm nm}^{-2})$	0.015	0.032	0.035	0.043	0.045

As noted above our experimental situation corresponds to the conformation of randomly and irreversibly grafted chains for which a theoretic model does not exist yet. To obtain the equilibrium layer thickness h_0 of the grafted hyaluronic acid film we therefore interpret our data in terms of the three simple theoretical models described above.

We start the analysis with the simple model of neutral adsorbed polymers as a first approximation of the polyelectrolyte layer in the high salt concentration limit (13). Figure 4 shows the fits of the theoretical potential composed of gravitational attraction and the polyelectrolyte induced repulsion modeled by adsorbed neutral polymers (13, 20) to the experimental data (dashed curves). The resulting equilibrium thicknesses of the hyaluronic acid layer at different salt concentrations are shown in Table 1. As mentioned in the theoretical section, this model accounts for a decreasing monomer density with the distance from the substrate surface, which is a reasonable assumption for our experimental situation.

Since the irreversible grafting as well as the charging of the monomers is neglected within this approach we analyze the hyaluronic acid layer also in terms of two simple models of polyelectrolyte brushes (12, 13), which assume that the charged chain ends of the polymers are irreversibly grafted to the surface at a fixed average distance. Both brush models are based on a constant segment density throughout the whole layer thickness and yield the surface coverage of the grafted polyelectrolyte film. It is important to notice that the measured surface coverage should be substantially lower than the real surface coverage because the bead mainly feels the dilute periphery of the hyaluronic acid layer. Therefore we treat the measured surface density as a variable parameter, denoted

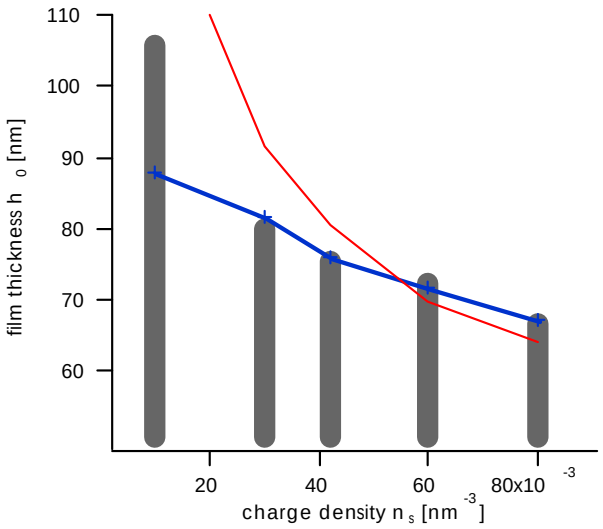

Fig. 5. Hyaluronic acid layer thickness plotted *versus* charge density of Na^+ ions within the film (grey bars). The black curve shows the theoretical prediction for the layer thickness in the high salt limit as suggested by Pincus [1] (*cf.* (7)). The grey curve shows an attempt to fit a curve $h_0 \propto n_s^{-1/2}$ according to the Ross and Pincus model [2] (*cf.* (9)).

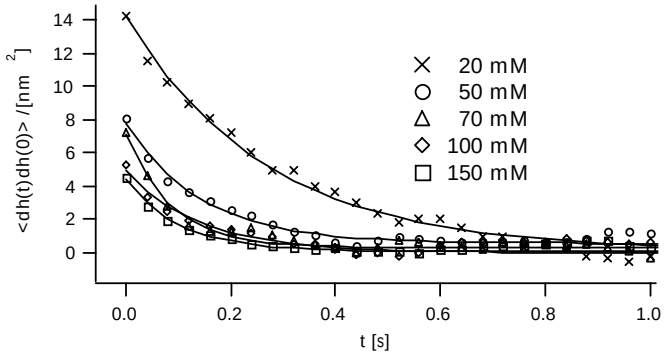

Fig. 6. Time autocorrelation functions of distance fluctuations of the sphere shown in Figure 4. Also shown are the best fits assuming single exponential decay according to (4).

Table 2. Parameters obtained by exponential fits to the autocorrelation functions of height fluctuations for different NaCl concentrations (*cf.* Fig. 6) are given.

NaCl conc./(mM)	20	50	70	100	150
$\langle dh^2\rangle/(nm^2)$	14.5	7.4	6.9	5.35	4.35
$V''/(k_BT/nm^2)$	0.07	0.13	0.144	0.187	0.23
$\tau/(s)$	0.64	0.14	0.1	0.11	0.1
$\eta_{eff}/(mPa\,s)$	7.55	3.45	3.54	3.56	3.64
$\xi_H/(nm)$	2.8	1.7	1.52	1.12	1.04

as effective surface coverage Γ_{eff} in the following. Figure 4 shows the best fits of the data points as obtained by assuming the effective gravitational potential and both polyelectrolyte brush models: the standard Pincus model for charged brushes (drawn curves) and the modified Ross and Pincus model for charged brushes (dotted curves). The results for the equilibrium thicknesses and the effective surface coverages, which slightly increase when the film is compressed, are shown in Table 1. In summary we found that the fitting curves of all three approaches exhibit remarkably good coincidence and the results for the equilibrium thickness are identical within experimental error for all salt concentrations.

In Figure 5 the equilibrium layer thickness h_0 is plotted *versus* the salt concentration (gray bars). The dashed line is the theoretical prediction of Pincus [1] for the condensation of grafted polyelectrolytes in the high salt concentration limit (7) evaluated with the observed effective surface coverages at a given salt concentration. For high salt concentrations this theoretical curve fits very well to the data yielding a contour length Na of 1 μm which is a reasonable value for the length of extended tails of the grafted hyaluronic acid layer. However, in the low salt regime this theoretical prediction deviates from the measured data by about 20%. This is quite reasonable because the polyelectrolyte chains are more stretched in the low salt regime and therefore the requirement of random coil structure might not be fulfilled. The drawn curve in Figure 5 is the best theoretical prediction of Ross and Pincus corresponding to a $h_0 \propto n_s^{-1/2}$ behavior (see (9)), which can be given with the measured film thicknesses and effective surface coverages. It is easily seen that the deviation of this model from the determined equilibrium thicknesses is unacceptable for all salt concentrations. In our experiment the grafted polyelectrolyte chains collapse with increasing salt concentration as power law, $h_0 \propto n_s^{-1/3}$. This behavior is in agreement to recent results for charged brushes of Guenoun *et al.* [27].

After condensation of the hyaluronic acid film we let the layer swell again by reducing the salt concentration to 20 mM NaCl as mentioned above. The resulting interaction potential is shown in Figure 4 (hatched curve). Compared to the initial curve measured also at a salt concentration of 20 mM NaCl before condensation, the curvature as well as the sphere-substrate distance at the potential minimum is reduced slightly. Thus the layer thickness is not restored completely. This might be due to entanglement of the polyelectrolyte chains during the condensation process.

We now discuss the influence of the hyaluronic acid cushion on the damping of the latex beads above the substrate. Figure 6 shows the autocorrelation functions evaluated from the height distributions in Figure 4. The elastic force constant V'' and the effective viscosity η_{eff} were determined by evaluating single exponential fits (4) to the data. The results for different salt concentrations are summarized in Table 2. It is seen that with increasing sphere-substrate distance the mean square displacement $\langle dh^2\rangle$ decreases corresponding to an increased elastic force constant V''. For all salt concentrations the effective viscosity is at least by a factor of 3 higher than that for the aqueous bulk solution ($\eta \approx 1$ mPa s). This increased effective viscosity indicates the influence of the grafted hyaluronic acid layer, which acts as an additional source of friction

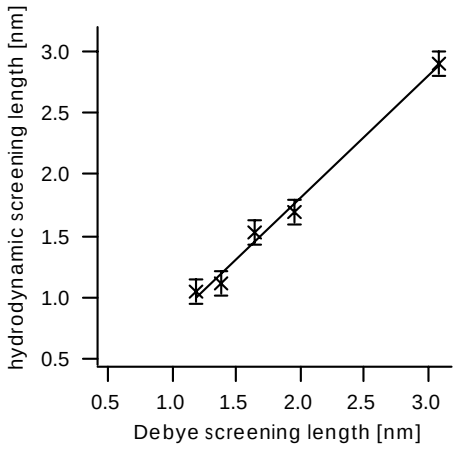

Fig. 7. Plot of the hydrodynamic screening length as obtained from (19) *versus* the Debye screening length. The line fit (drawn line) has a slope of nearly 45 degrees corresponding to identical scaling of both characteristic length scales of the grafted hyaluronic acid film.

to the streaming water. Furthermore, Table 2 shows the hydrodynamic screening lengths calculated from (19). The decrease of ξ_H with increasing salt concentrations is a consequence of the reduction of the Debye screening length. In Figure 7 we plotted the hydrodynamic decay length *versus* the Debye screening length to compare both typical length scales of the system. The straight line fitted to the data clearly demonstrates the linear dependence of these two quantities. Moreover the slope of the fit which is nearly 45 degrees shows that the hydrodynamic screening length and the Debye screening length differ only by a small constant offset.

4.2 The influence of divalent ions

In the remaining part of this section we report on the influence of divalent Ca^{2+} ions on the state of a grafted hyaluronic layer. We carried out experiments with salt concentrations of 5, 10, and 50 mM $CaCl_2$. The interaction potentials $V(h)$ were measured as described before and are shown in Figure 8 while the mean sphere-substrate distances, the mean square height fluctuations and the elastic force constants are listed in Table 3. The effect of divalent cations is much more dramatic than of monovalent cations. At a $CaCl_2$ concentration of 50 mM the layer thickness is reduced nearly by a factor of two compared to 5 mM $CaCl_2$. The increased condensation of the hyaluronic acid film by Ca^{2+} ions compared to the influence of Na^+ ions can be understood by the increased screening of divalent ions. Note that the charge number z enters as a quadratic term into the Debye screening length. In addition, the situation appears to be more difficult because Ca^{2+} ions (in contrast to Na^+ ions) are able to form local chelate complexes between the carboxyl groups of the hyaluronic acid chains [12]. A so-called egg-box configuration is formed which leads to local crosslinking and we should expect a significant hysteresis in the condensation-

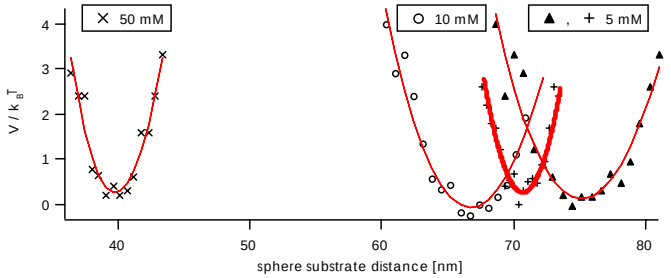

Fig. 8. Interaction potentials of a latex bead hovering over a hyaluronic acid layer in solutions with $CaCl_2$ concentrations of 5, 10, and 50 mM. The solid curves are only drawn to guide the eye and do not correspond to theoretical fits. The hatched curve is the interaction potential measured in a 5 mM $CaCl_2$ solution after condensation and swelling of the layer.

Table 3. Mean sphere-substrate distances and parameters of the exponential fits to the autocorrelation functions of height fluctuations for different $CaCl_2$ concentrations.

$CaCl_2$ conc./(mM)	5	10	50
$\langle h\rangle$/(nm)	75.3	66.7	39.8
$\langle \mathrm{d}h^2\rangle$/(nm^2)	4.8	2.9	0.8
$V''/(k_BT/\mathrm{nm}^2)$	0.08	0.14	0.5
τ/(s)	0.12	0.09	0.1
η_{eff}/(mPa s)	1.81	2.1	4.97

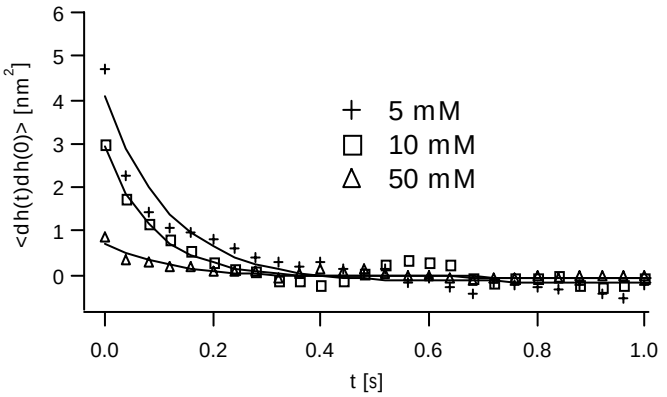

Fig. 9. Time autocorrelation functions of distance fluctuations corresponding to the potentials in Figure 8. Also shown are single exponential fits according to (4).

swelling behavior. Surprisingly, the interaction potential of the re-swollen hyaluronic acid layer (*cf.* Fig. 8, hatched curve) exhibits only a small shift with respect to the potential curve observed before condensation. Therefore we can not distinguish between simple entanglement effects and Ca^{2+}-induced conformational changes of the polyelectrolyte chains in this experiment.

Figure 9 shows the autocorrelation functions corresponding to the Ca^{2+} concentrations studied in Figure 8. The resulting mean square amplitudes $\langle \mathrm{d}h^2\rangle$ and decay times τ as well as the fitted elastic force constants V'' and effective viscosities η_{eff} are shown in Table 3. Both the elastic force constants and the effective viscosities are

increased with increasing $CaCl_2$ concentration. Qualitatively there is no difference between these results and the results for monovalent ions. The hardening of the supported hyaluronic acid cushion is due to the enhanced monomer concentration resulting in a reduced layer thickness.

5 Conclusions

We investigated the influence of monovalent Na^+ and divalent Ca^{2+} ions on the viscoelastic properties of a grafted hyaluronic acid layer. The effect of monovalent ions on the swelling behavior of grafted hyaluronic acid is described quantitatively by different theoretical approaches of polyelectrolyte brushes and neutral adsorbed polymers. In particular the equilibrium layer thickness, determined by applying these different theoretical models are identical within experimental error. This result indicates that the data evaluation is not very sensitive to the special theoretical model, which is used for the fit. Therefore it is possible to model the randomly grafted hyaluronic acid layer as a simple polyelectrolyte brush. Within this approximation it is possible to calculate an effective surface coverage of the grafted film. Interestingly, our results can distinguish between the two different brush models concerning the dependence of the swelling behavior on the salt screening. The film thickness data in our experiment clearly support the $h_0 \propto n_s^{-1/3}$ behavior in the high salt limit.

At this point a remark should be made about the internal structure of the hyaluronic acid layer. The configuration of hyaluronic acid in solution is supposed to be not entirely random but is expected to involve some helical sections [28]. However, because of the above results we expect no dramatic effect on the general swelling behavior. Concerning this basic assumption we also refer to the original work of Rabin *et al.* [21] and Pincus [1]. As discussed by these authors the forces are dominated by the local polyelectrolyte concentration and do not depend on factors such as the conformation of the polyelectrolyte chains or their degree of penetration. Nevertheless, the layer structure and the monomer density profile are important physical parameters to characterize the randomly grafted hyaluronic acid film. For this purpose other physical techniques like neutron reflectometry should be used for a more detailed investigation of the microscopic layer structure. Then it would be possible to distinguish between the different theoretical models for the description of the swelling behavior of ultrathin hyaluronic acid films.

Our results demonstrate that surfaces can be stabilized effectively by ultrathin hyaluronic acid films due to its elastic properties. Even at salt concentrations similar or higher than physiological values the polyelectrolyte film does not collapse appreciably. This result is in striking contrast to repulsive electrostatic forces between bare surfaces, which are screened out already at very short distances of a few Å at similar salt concentrations. On the other hand hyaluronic acid exhibits a distinctive swelling behavior that can be varied by the adjustment of the ionic strength. Interestingly the swelling and condensation of the grafted layer is nearly reversible and occurs spontaneously within time resolution of our experiments, which is in the range of minutes. This indicates that the dynamics of the swelling process in our experiments is determined by the time needed for the exchange of the solvent. The fast mechanism of salt dependent swelling of hyaluronic acid films might play an important role for the rapid control of the swollen state of the extracellular matrix.

In order to interpret the dynamics of the swelling and condensation process we modeled the hyaluronic acid layer as an elastic Brinkmann medium with an effective pore size. The macroscopic condensation was described microscopically in terms of contraction of the pores due to enhanced screening with increased salt concentration. The meshsize turned out to be the characteristic length scale of the grafted hyaluronic acid film in the high salt limit and it can be interpreted both as hydrodynamic screening length and as Debye screening length.

We are grateful to the Wacker Chemitronic GmbH, Burghausen, Germany for providing thermally oxidized silicon wafers as a gift. This work was supported by the Deutsche Forschungsgemeinschaft (DFG SA 246/27-1) and the Fond der Chemischen Industrie.

References

1. P. Pincus, Macromolecules **24**, 2912 (1991).
2. R.S. Ross, P. Pincus, Macromolecules **25**, 2177 (1992).
3. P.J. de Gennes, Adv. Coll. Int. Sci. **27**, 189 (1987).
4. E.D. Hay, *Cell Biology of Extracellular Matrix*, edited by E.D. Hay (Plenum Press, New York, 1991), vol. 2.
5. B.P. Toole, *Cell Biology of Extracellular Matrix*, edited by E.D. Hay (Plenum Press, New York, 1991), vol. 2.
6. E.A. Balazs, *Healon: A Guide to its Use in Opthalimc Surgery*, edited by D. Miller, R. Stegmann (Wiley, New York, 1983).
7. B. Alberts, D. Bray, J. Lewis, R. Raff, K. Roberts, J.D. Watson, *Molecular Biology of the Cell* (Garland, New York, 1983).
8. J. Rädler, E. Sackmann, Langmuir **8**, 848 (1992).
9. M. Kühner, E. Sackmann, Langmuir **12**, 4866 (1996).
10. F.R. Hallet, A.L. Gray, Biochim. Biophys. Acta **343**, 648 (1974).
11. M. Rinaudo, M. Milas, N. Jouon, R. Borsali, Polymer **34**, 3710 (1993).
12. L. Fransson, *The Polysaccharides*, edited by G.O. Aspinall (Academic Press, Toronto, 1985), vol. 3.
13. E. Fouissac, M. Milas, M. Rinaudo, R. Borsali, Macromolecules **25**, 5613 (1992).
14. G.U. Glück, Diploma Thesis, Johannes Gutenberg Universität, Mainz, 1993.
15. G. Elender, M. Kühner, E. Sackmann, Biosensors Bioelectron. **11**, 565 (1996).

16. E.T. Vandenberg, L. Bertilsson, B. Liedberg, K. Uvdal, R. Erlandsson, H. Elwing, I. Lundström, J. Coll. Int. Sci. **147**, 103 (1991).
17. R.C. Weast, *Handbook of Chemistry and Physics* (The Chemical Rubber Co. (CRC), Cleveland, 1971).
18. A. Zilker, H. Engelhardt, E. Sackmann, J. Phys. France **48**, 2139 (1987).
19. O. Reynolds, Trans. R. Soc. London **177**, 157 (1886).
20. G.S. Manning, J. Chem. Phys. **51** (3), 924 (1969).
21. Y. Rabin, G.H. Fredrickson, P. Pincus, Langmuir **7**, 2428 (1991).
22. J.N. Israelachvili, R.M.J. Pashley, Colloid Interface Sci. **2**, 501 (1984).
23. H.C. Brinkmann, Appl. Sci. Res. A **1**, 27 (1947).
24. G.H. Fredrickson, P. Pincus, Langmuir **7**, 786 (1991).
25. E.S. Shaqfeh, G.H. Fredrickson, Phys. Fluids A **2**, 7 (1990).
26. E.J. Verwey, J.T. Overbeck, *Theory of the Stability of Lyophobic Colloids* (Elsevier, Amsterdam, 1948).
27. P. Guenoun, A. Schlachli, D. Sentenac, J.W. Mays, J.J. Benattar, Phys. Rev. Lett. **74**, 3628 (1995).
28. W.D. Comper, T.C. Laurent, Physiol. Rev. **58** (1978).